Sound & Vibration 2026, 60(5), 4627.
doi: https://doi.org/10.59400/sv4627

Article

Analytical design and multi-parameter optimization of micro-perforated double-panel partitions for normal-incidence broadband sound transmission loss

Tahir Muhammad Ali[1], Yogeesh Nijalingappa[2,3,4,*], Asokan Vasudevan[4], Rajashree Jain[5], P. William[6,7]

[1] Department of Computer Science, Gulf University for Sciences and Technology, Safat 13060, Kuwait
[2] Department of Mathematics, Government First Grade College, Tumkur 572102, India
[3] Mathematics and Natural Sciences, Gulf University for Science and Technology, Safat 13060, Kuwait
[4] Faculty of Business and Communications, INTI International University, Nilai 71800, Malaysia
[5] Symbiosis Institute of Computer Studies and Research, Symbiosis International (Deemed University), Pune 411016, India
[6] School of Computer Science and Technology, Karunya Institute of Technology and Sciences (Deemed University), Coimbatore 641114, India
[7] Centre for Research and Consultancy, UNITAR International University, Petaling Jaya 47301, Malaysia
*** Corresponding author:** Yogeesh Nijalingappa, yogeesh.n@ka.gov.in

CITATION

Ali TM, Nijalingappa Y, Vasudevan A, et al. Analytical design and multi-parameter optimization of micro-perforated double-panel partitions for normal-incidence broadband sound transmission loss. Sound & Vibration. 2026; 60(5): 4627. https://doi.org/10.59400/sv4627

ARTICLE INFO

Received: 6 July 2026
Revised: 21 July 2026
Accepted: 27 July 2026
Available online: 17 August 2026

Abstract: An analytical and computation-based framework is presented for designing a micro-perforated double-panel partition with improved broadband sound transmission loss. The study combines closed-form expressions, transfer matrices, dimensionless design parameters and tabulated numerical values to support practical acoustic design. In the present work, a thin micro-perforated panel is asymmetrically inserted into the cavity spanning between two parallel panels that are separated by an air cavity forming coupled resonant mechanisms. This normal-incidence transfer-matrix model is composed of panel impedances, cavity propagation matrices and Maa-type micro-perforate impedance formulas. A local Helmholtz-type estimate of transmission loss and the mass-air-mass resonance are stated explicitly, followed by a simultaneous optimization of hole diameter, perforation ratio, micro-perforated sheet thickness and cavity split over a target frequency band. Over the 100–2,000 Hz band, the optimized asymmetric micro-perforated design improves the weighted average transmission loss by 6.49 dB and the arithmetic band-average transmission loss by 9.33 dB relative to the baseline double panel, with the strongest gains occurring in the upper octave bands. Parameter sweeps show that smaller perforations and slightly asymmetric cavity splits yield the best broadband trade-off for this case. Because the optimum occurs at the stated lower manufacturing bounds, it is interpreted as a constrained design result. Diffuse-field incidence, elastic plate dynamics, manufacturing tolerances, and experimental validation remain for future work.

Keywords: sound transmission loss; double-panel partition; micro-perforated panel; transfer-matrix model; broadband optimization

1. Introduction

A double-panel partition with lightweight face sheets and an enclosed air cavity can provide higher sound insulation than a comparable single panel while remaining relatively easy to assemble by bonding or bolting. Its disadvantage is also well known: the air layer trapped between the two panels can create a mass-air-mass resonance and, in the low-to-mid-frequency range, can produce a deep dip in transmission loss. As a result the design must not only maximize the average transmission loss but also control the location, depth and bandwidth of this dip while retaining stable performance in high frequencies. This is where micro-perforated panels (MPPs) are especially useful: they can provide properly damped or reactive frequency-selective resistance without any need for fibrous fill. With good tunability through hole diameter, perforation ratio, sheet thickness or cavity depth, they have become one of the most widely-used tools for this purpose in recent years. For example, recent reviews and analytical studies have demonstrated their roles in sound absorption, enclosure noise control, multilayer vibroacoustics and compact noise-mitigation treatments [1–5].

A major advantage of MPP-based structures is that their performance can be represented by compact impedance models [6]. Because of this, there is a rich theoretical tradition in multilayer absorbers, energy loss through perforated patterns, barrier-tube analysis, and vibroacoustic transfer matrices [7–11]. Newer research has expanded the design scope through three-dimensional printing, unconventional open-area shapes, wavy or spatially variable MPP layouts, and multifunctional acoustic metamaterials [12–16]. Elsewhere in the vibroacoustic literature, studies on double-panel-cavity systems, stiffened partitions, panel laminates, and cavity-coupled structures show the need for transparent design tools that can handle increasingly complex systems [17–20]. Despite this progress, however, practical MPP-insulated double-panel design remains difficult because the design parameters are strongly coupled. Changing perforation ratio has a similarly dual effect. The internal position of the MPP in the cavity influences how the local resonator couples with global mass-air-mass motion, but it has often been treated as a fixed geometric quantity rather than an optimization variable. Many studies consider absorption or specific finite-element implementations, but fewer provide a compact analytical treatment that transforms these coupled parameters into design maps for broadband transmission loss [21–25]. Complementary absorption, transmission-loss, enclosure, double-leaf, and cavity-coupling studies are cited in some researches [26–29].

The present study addresses this gap in a mathematical and numerically explicit way. A normal-incidence transfer-matrix model of the double-panel partition with the inserted MPP is developed. Panel impedance is modeled via a thin-plate mass law with loss factor, cavity propagation is analytically represented and the MPP impedance is expressed using a Maa-type expression that accounts for both resistive and inertial contributions. The total transmission coefficient and transmission loss are derived explicitly based on these building blocks. A broadband optimization is then performed over hole diameter d_h, perforation ratio ϕ, MPP thickness t and cavity split $\frac{d_1}{D}$, while the total cavity depth D is held constant. The study quantitatively examines the improvement of an asymmetric MPP relative to a bare double panel and a symmetric insertion, identifies the most sensitive parameter for weighted average transmission loss, and derives compact dimensionless indicators that explain the optimum.

The focus is on practical analytical design rather than complete multi-physics simulation. By confining attention to normal incidence and thin-panel impedance, the model is simple enough to elucidate parameter trends quite effectively. At the same time, the resulting formulas are fully consistent with standard acoustic transfer-matrix practice and are rich enough to produce useful optimization and sensitivity information.

The study is therefore aligned with the type of sound and vibration study that emphasizes physically grounded modeling, numerical tables, and transferable design rules.

The assumptions of normal incidence, plane-wave propagation and thin-panel impedance are therefore stated explicitly as modeling limitations and as the basis for a transparent early-stage design tool.

2. Transfer-matrix formulation for the micro-perforated double panel

2.1. Constituent matrices

The system considered is shown in **Figure 1**. Two parallel face panels with areal masses m_1 and m_2 enclose a total cavity depth D. An MPP of thickness t, perforation ratio ϕ, and hole diameter d_h is inserted inside the cavity at distance d_1 from the source panel and $d_2 = D - d_1$ from the receiving panel. Under normal incidence and plane-wave propagation, the acoustic state vector is written as

$$s(x) = \begin{bmatrix} p(x) \\ u(x) \end{bmatrix},$$

here, p denotes acoustic pressure, u denotes particle velocity. $k = \frac{\omega}{c_0}$ is the acoustic wavenumber, $Z_0 = \rho_0\, c_0$ is the characteristic impedance of air, ρ_0 is air density and c_0 is the speed of sound.

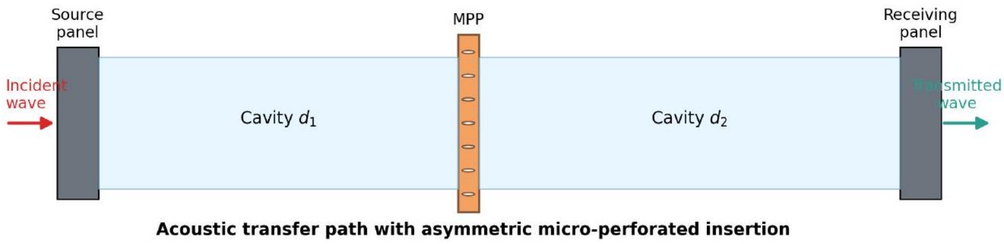

Figure 1. Schematic of the analytical model: Two face panels bound an air cavity of total depth D, and a microperforated panel is inserted asymmetrically so that $D = d_1 + d_2$.

For a homogeneous air layer of thickness d, the acoustic state vector at x is related to that at $x + d$ by

$$s(x) = T_c(d)s(x + d),$$

where $T_c(d)$ is the standard transfer matrix:

$$\mathrm{T}_c(d) = \begin{bmatrix} \cos(kd) & iZ_0 \sin(kd) \\ i \sin(kd)/Z_0 & \cos(kd) \end{bmatrix},\ k = \frac{2\pi f}{c_0},\ Z_0 = \rho_0 c_0$$

The state is propagated from the receiving side toward the source side using the $e^{i\omega t}$ convention; under $e^{-i\omega t}$, both off-diagonal signs reverse consistently.

A thin panel or thin perforated sheet acting as a lumped series impedance Z is represented by

$$\mathrm{T}_p(Z) = \begin{bmatrix} 1 & Z \\ 0 & 1 \end{bmatrix}$$

For the two face panels, a thin-plate mass-law impedance with a small structural loss term is used:

$$Z_{p,j} = \eta_p \omega m_j + i\omega m_j,\ j = 1, 2,$$

where $\omega = 2\pi f$ and η_p is a phenomenological damping coefficient. This full form is sufficient for a normal-incidence design study that is calculation-focused and comparative rather than precise in high-frequency plate mode predictions.

The panel loss-factor symbol is now consistent with **Table 1**.

Table 1. Acoustic constants, panel properties, and optimization bounds used in the MPP double-panel study.

Parameter	Symbol	Value
Air density	ρ_0	1.21 kg/m^3
Speed of sound	c_0	343 m/s
Dynamic viscosity of air	η	1.84 × 10^{-5} Pa s
Characteristic impedance of air	Z_0	415 Pa s/m
Areal mass of source panel	m_1	2.70 kg/m^2
Areal mass of receiving panel	m_2	2.70 kg/m^2
Panel loss factor coefficient	η_p	0.03
Total cavity depth	D	80 mm
Frequency band	f	100–2,000 Hz
Search range of hole diameter	d_h	0.25–0.70 mm
Search range of perforation ratio	ϕ	0.006–0.018
Search range of upstream cavity depth	d_1	20–60 mm
Discrete panel thicknesses	t	0.40, 0.60, 0.80, 1.00 mm

2.2. Maa-type impedance of the micro-perforated panel

The MPP impedance is expressed in the standard resistive-reactive form

$$Z_m = R_m + iX_m$$

Following a Maa-type approximation, the resistive component is

$$R_m = \frac{32\eta_0 t}{\phi d_h^2}\left[\sqrt{1+\frac{x^2}{32}} + \frac{\sqrt{2}}{32}x\frac{d_h}{t}\right],\ x = d_h\sqrt{\frac{\omega\rho_0}{4\eta_0}}$$

and the reactive component is

$$X_m = \frac{\omega\rho_0 t}{\phi}\left[1 + \frac{1}{\sqrt{9 + x^2/2}} + 0.85\frac{d_h}{t}\right]$$

These expressions account for both the viscous drag of the narrow holes and the end-corrected inertial mass of the air slugs in and nearby the perforations. They also immediately demonstrate why d_h, ϕ, and t are strongly interrelated. A decrease in hole diameter increases the resistance roughly as $1/d_h^2$, and a reduction of perforation ratio also inflates both resistance and reactance through the factor $1/\phi$. A thicker MPP sheet increases inertial reactance, which can improve low-frequency tuning when it is matched with the cavity depth; however, excessive thickness may create high reactance and narrow the effective attenuation band.

2.3. Overall transmission coefficient

The total transfer matrix of the partition is written as follows

$$\mathrm{T} = \mathrm{T}_p\left(Z_{p,1}\right)\mathrm{T}_c\left(d_1\right)\mathrm{T}_p\left(Z_m\right)\mathrm{T}_c\left(d_2\right)\mathrm{T}_p\left(Z_{p,2}\right) = \begin{bmatrix} A & B \\ C & D \end{bmatrix}$$

Now, assuming the incident as well as transmitted media are both air, the normal-incidence transmission coefficient is

$$\tau = \frac{2}{A + B/Z_0 + CZ_0 + D},$$

Applying the incident, reflected, and transmitted pressure–velocity boundary states and eliminating the reflected pressure gives

$$2p_i = (A + \frac{B}{Z_0} + CZ_0 + D)p_t.$$

Hence the stated coefficient requires identical incident and receiving media, but it does not require geometric symmetry. The corresponding power coefficient is $T = |\tau|^2$, which recovers the stated transmission-loss equation.

And the corresponding transmission loss is

$$TL = -20\log_{10}|\tau|.$$

This formulation is computationally convenient because any change in design only changes a small subset of scalar parameters which leads to the same matrix algebra. Similarly, this same framework is well suited for parameter sweeps as well as numerical optimization.

2.4. Frequencies and dimensionless groups

Two reference frequencies are particularly useful for interpreting the results. The first is the mass-air-mass resonance of the bare double panel,

$$f_{\mathrm{mam}} = \frac{c_0}{2\pi}\sqrt{\frac{\rho_0}{D}\left(\frac{1}{m_1} + \frac{1}{m_2}\right)}.$$

The second is a Helmholtz-type estimate associated with the perforated insert,

$$f_H \approx \frac{c_0}{2\pi}\sqrt{\frac{\phi}{D\left(t + 0.85d_h\right)}}.$$

Although the exact coupled-system behavior depends on the full transfer matrix rather than on these formulas alone, they are extremely useful for interpreting design trends. In the present study the baseline mass-air-mass resonance is 182.72 Hz, while the optimized MPP design yields $f_H \approx 429.34$ Hz. This separation helps explain why the optimized structure both moderates the main low-frequency dip and generates strong improvement through the mid-to-high portion of the band.

Direct substitution of the stated panel masses, cavity depth, air density, and sound speed gives 182.72 Hz, confirming that the 1.73 dB minimum is the modeled resonance dip; no leakage or bypass path is included.

The asymmetry is one of the key design variables in the optimization study. The perforation geometry used in the design sweep is illustrated in **Figure 2**.

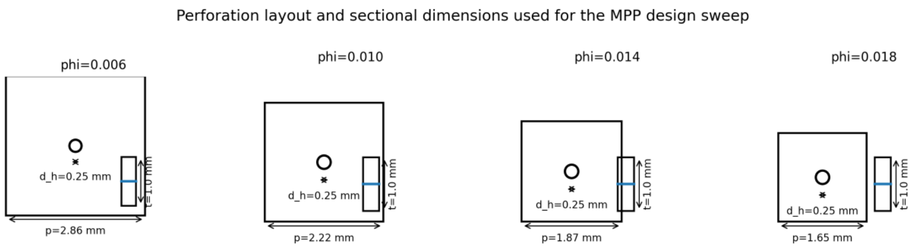

Figure 2. Perforation detail used in the design sweep. The front-view pitch p is calculated from $\phi = \pi\, d_h^2/(4p^2)$, and the sectional view shows the hole diameter d_h through the MPP thickness t.

3. Optimization problem and numerical settings

The design objective is a weighted average transmission loss over $100-2,000\,\mathrm{Hz}$,

$$J = \frac{\int_{f_1}^{f_2} w(f) TL(f) df}{\int_{f_1}^{f_2} w(f) df},\ w(f) = \frac{1}{1 + f/700},$$

with $f_1 = 100\,\mathrm{Hz}$ and $f_2 = 2,000\,\mathrm{Hz}$. The weighting function gives slightly higher emphasis to the low and mid-low band, where double-panel systems are most vulnerable, without completely neglecting the upper part of the spectrum. This choice is more informative than a simple arithmetic average when one wishes to design around the mass-air-mass dip.

The arithmetic average *TL* is computed with uniform frequency weighting, whereas the weighted average *TL* uses $w(f)$ to place greater emphasis on the vulnerable low and mid-low frequency region; this distinction explains why **Table 2** reports both average and weighted-average values.

Table 2. Baseline partition vs. a symmetric MPP insertion vs. optimized asymmetric design.

Configuration	Minimum TL (dB)	Average TL (dB)	Weighted average TL (dB)	125 Hz	250 Hz	500 Hz	1,000 Hz	2,000 Hz
Double panel only	1.73	51.27	45.70	7.25	19.90	42.79	58.72	62.69
Symmetric MPP baseline	1.77	52.68	45.66	7.40	19.63	40.69	52.84	75.70
Optimized asymmetric MPP	2.44	60.60	52.19	8.14	19.84	42.28	65.95	84.44

The baseline double panel uses $m_1 = m_2 = 2.7\mathrm{kg\,m^{-2}}$ and total cavity depth $D = 80$ mm. Two reference comparison cases are evaluated: a bare double panel with no MPP, and a symmetric MPP insertion using $d_h = 0.50$ mm, $\phi = 0.012,\ t = 0.8$ mm, and $d_1 = d_2 = 40$ mm. The optimization search then varies d_h, ϕ, t, and d_1 over the ranges given in **Table 1**. The best configuration found for the present model uses the smallest hole diameter in the search set, the smallest perforation ratio, the thickest MPP, and a moderately asymmetric cavity split.

The lower limits of 0.25 mm hole diameter and 0.006 perforation ratio were retained as manufacturing-feasible bounds because smaller values increase drilling tolerance, blockage, and viscous-property uncertainty; the reported result is therefore a constrained boundary optimum.

The upstream cavity depth was sampled at 0.133 mm intervals, so 33.33 mm is a computational grid value and should be interpreted practically as approximately 33.3 mm.

These trends already suggest the governing physics: smaller holes and lower perforation ratio increase viscous resistance and acoustic dissipation. A thicker sheet increases the neck effective mass and lowers the local resonance. Moreover, placing the MPP away from the cavity mid-plane allows the local perforate resonance to interact more effectively with the global cavity motion than a strictly symmetric standing-wave arrangement.

4. Results

4.1. Baseline, symmetric, and optimized configurations

Table 2 and **Figure 3** compare the three principal configurations. The minimum TL of the double panel with no additional treatment is 1.73 dB, while its weighted average TL is 45.70 dB. The symmetric MPP baseline slightly lowers the weighted average to 45.66 dB because its gain near 2,000 Hz is offset by lower values in the more heavily weighted 250–1,000 Hz range. The optimized asymmetric MPP design achieves a significantly better minimum transmission loss of 2.44 dB, an arithmetic average TL of 60.60 dB, and a weighted average of 52.19 dB.

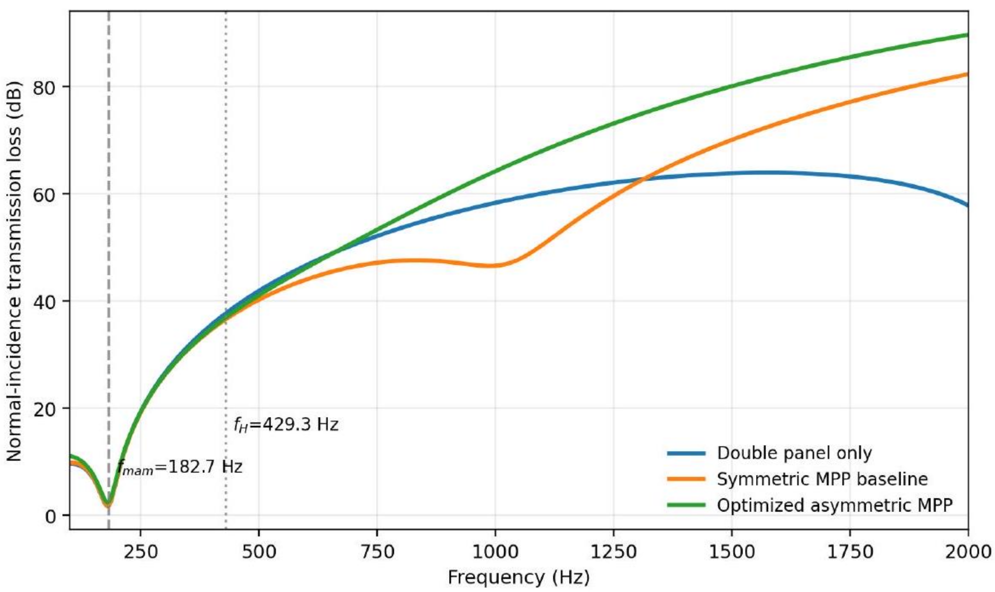

Figure 3. Transmission-loss curves for the three principal configurations.

The optimized design shows a weighted-average improvement of 6.49 dB compared to the double panel without an MPP insert. In acoustical engineering, such an enhancement is substantial because it conveys broadband spectral benefit rather than a suppression of only one very narrow notch. This redistribution is also confirmed by the octave-band behavior. The optimized design shows an improvement of about 7.23 dB at the 1,000 Hz band and 21.75 dB at the 2,000 Hz band compared with just the bare double panel one. The 250 Hz and 500 Hz bands remain difficult at all, but this is expected because they fall within the transition regime between global mass-air-mass behaviour and local perforated tuning. But you net off much better.

Figure 3 indicates how this improvement is achieved. Mostly all three systems shield insignificantly around the mass-air-mass resonance, yet the MPP of asymmetric enhancement gives more balanced recovery at this frequency. The symmetric MPP design excels at high frequency but the optimized asymmetric system has a superior mid-band slope. More specifically, asymmetry is more than simply a cosmetic change; it modifies the coupling of cavity segments increasing the attenuation bandwidth. The derived frequencies and optimized geometric values are summarized in **Table 3**.

Table 3. Derived characteristic frequencies and optimized geometric values.

Quantity	Symbol	Value
Mass-air-mass resonance	f_{mam}	182.72 Hz
Helmholtz estimate for optimum MPP	f_H	429.34 Hz
Optimal hole diameter	d_h	0.25 mm
Optimal perforation ratio	ϕ	0.006
Optimal MPP thickness	t	1.00 mm
Optimal upstream cavity depth	d_1	33.33 mm
Optimal downstream cavity depth	d_2	46.67 mm
Optimal cavity split	$\chi = d_1/D$	0.4167

The vertical dashed line indicates the mass-air-mass resonance of the bare double panel, whereas the dotted line represents a Helmholtz-type prediction for the optimized MPP branch. The corresponding octave-band comparison is shown in **Figure 4**.

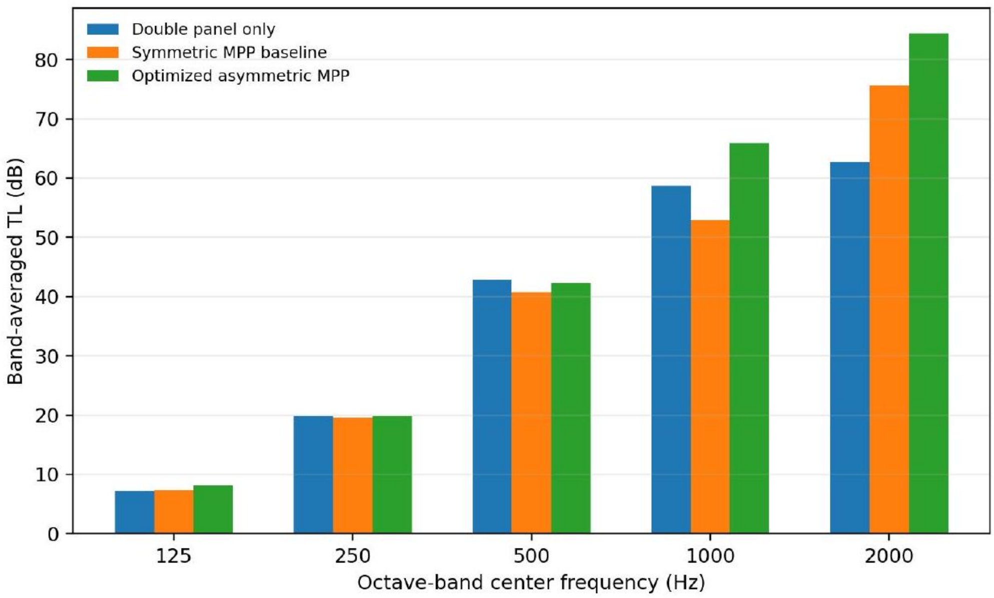

Figure 4. Octave-band comparison of the three configurations.

The optimized asymmetric MPP, while maintaining a low-frequency trend of the bare system, significantly enhances upper-octave transmission-loss values.

4.2. Perforation ratio and hole diameter

The weighted average transmission loss as a function of hole address, four hole diameters and split between two symmetric cavities (constant) is summarized in **Figure 5**. The pattern is obvious: smaller perforation ratios yield higher weighted average TL within the valid search range with greater advantages observed at small hole diameters. This is evident from the Maa impedance expressions. Reducing ϕ increases both the resistive and reactive components of the MPP impedance. Here, the augmented resistive component is indeed dominant because it dissipates a greater amount of acoustic energy and remains below the operational bandwidth limit imposed by reactance augmentation.

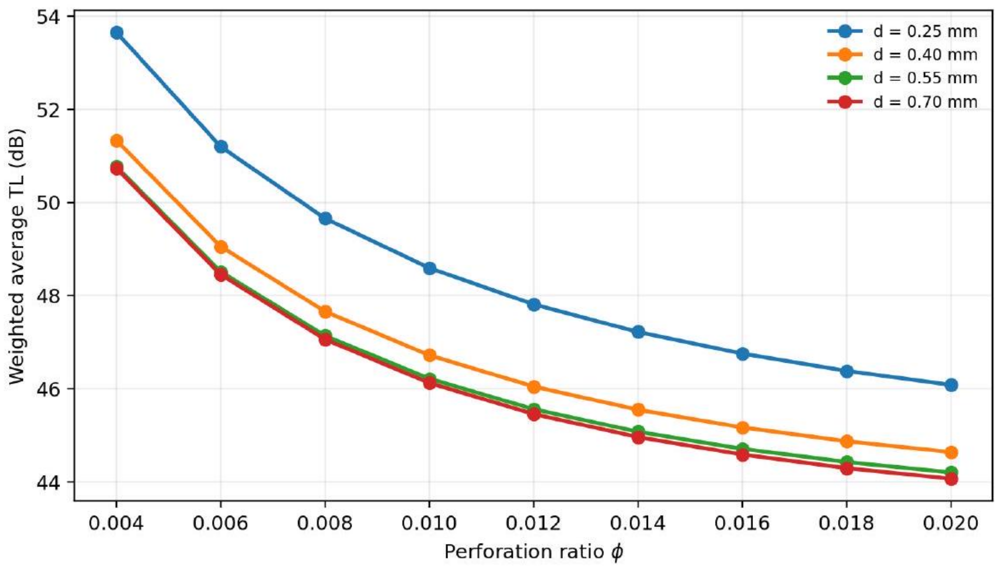

Figure 5. Weighted average transmission loss versus perforation ratio for several hole diameters.

Diameter is another significant shape feature. At, the average transmission loss decreases from around 53.6 dB for mm to about 50.7 dB for mm. Sensitivity does decrease with somewhat, but it remains large across a substantial range. This means that precision manufacturing with a small punch is an inherent design lever rather than an afterthought. Such a mapping specifically defines an otherwise qualitative statement even more tractably, thus making such data very important for analytically driven sound and vibration design in the paper.

Within the design window analysed, smaller holes and smaller perforation ratios produce better broadband response.

4.3. Asymmetry of cavity split influence

The upstream cavity depth, though often neglected in practical design, has a significant and non-monotonic influence as shown in **Figure 6**. The weighted average transmission loss is maximized for every perforation ratio displayed when is around 35–40 mm, at a corresponding cavity split ratio of roughly 0.44–0.50 for the fixed values chosen in the sweep. Once again the best split shifts down to ϕ, with the final optimum using t = 1.0 mm and the minimum hole diameter in the search range. This moderate asymmetry indicates that strict mid-plane placement can force the two cavity compliances to act too similarly, whereas an off-centre insert creates unequal upstream and downstream acoustic compliances that broaden the resonance coupling.

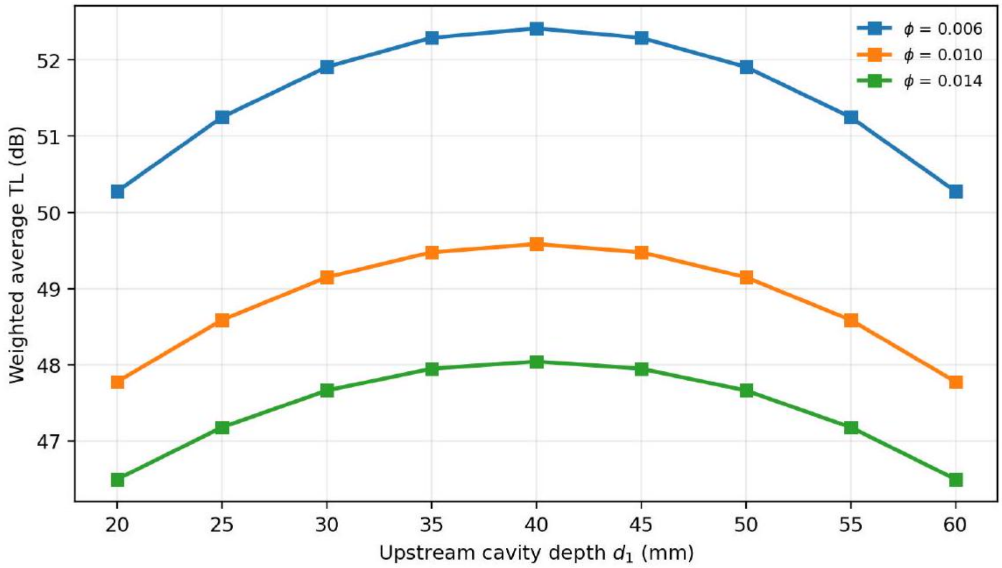

Figure 6. Weighted average transmission loss versus upstream cavity depth.

The shape of the curves in **Figure 6** is also significant. If the insert is too close to either face panel, performance will drop. In physical terms, one cavity becomes too compliant and the other cavity becomes too stiff, losing broadband balance in a coupled resonator. This result, thus, translates to a pragmatic design rule from the present study that one should start with $0.40 \leq \chi \leq 0.50$ rather than strict symmetry.

Support for this mechanism appears in the parametric results in **Figure 6**: For all perforation ratios plotted, broad maximum exists at non-exact mid-plane, suggesting that moderate asymmetry may lead to improved broadband coupling, not just shift of one resonance point.

We note that for the present configuration, moderate asymmetry is better than exact symmetry (as inferred from the broad maxima).

5. Sensitivity analysis and compact design interpretation

5.1. Finite-difference sensitivity

For the optimal point, a finite-difference sensitivity analysis was conducted using one-sided perturbations around the reported optimum. The perturbation magnitudes were $\Delta d_h = 0.025$ mm, $\Delta\phi = 0.0006$, $\Delta d_1 = 0.133$ mm and $\Delta t = 0.10$ mm. For each variable θ_i, the reported value was calculated from $S_i = \left[\frac{J(+) - J(-)}{2J0}\right](\theta_i/\Delta\theta_i)$, where $J0$ is the objective at the optimum and $J(-)$, $J(+)$ are the objective values at the lower and upper perturbations. Of the four optimized variables, the cavity split exhibits the highest positive normalized sensitivity, indicating that a shift in insert location most strongly affects weighted average transmission loss. The MPP thickness is also influential, while hole diameter and perforation ratio show negative sensitivities that are consistent with the benefit of smaller d_h and smaller ϕ.

These values are local screening slopes rather than manufacturing tolerances; linearity beyond one increment was not verified, and placement sensitivity should be confirmed using several step sizes before practical use.

The hole-diameter, perforation-ratio, and thickness increments are 10% of their optimal values, whereas the placement increment is one numerical grid interval.

The magnitude hierarchy is instructive. In an engineering workflow in which some of the parameters are fixed by manufacturing constraints, insert placement and thickness should be prioritized first, followed by achieving the smallest possible diameter and perforation ratio. Conversely, if a supplier has tooling that locks hole diameter and perforation ratio, then optimizing the cavity split can still recover much of the lost performance. The finite-difference values are reported in **Table 4**, and their normalized comparison is shown in **Figure 7**.

Table 4. Finite-difference sensitivity-weighted average transmission loss in the neighbourhood of optima.

Parameter	J(−) (dB)	J0 (dB)	J(+) (dB)	Normalized sensitivity
d_h	53.004	52.192	51.554	−0.139
ϕ	52.835	52.192	51.628	−0.116
d_1	51.837	52.192	52.380	1.302
t	50.985	52.192	53.250	0.217

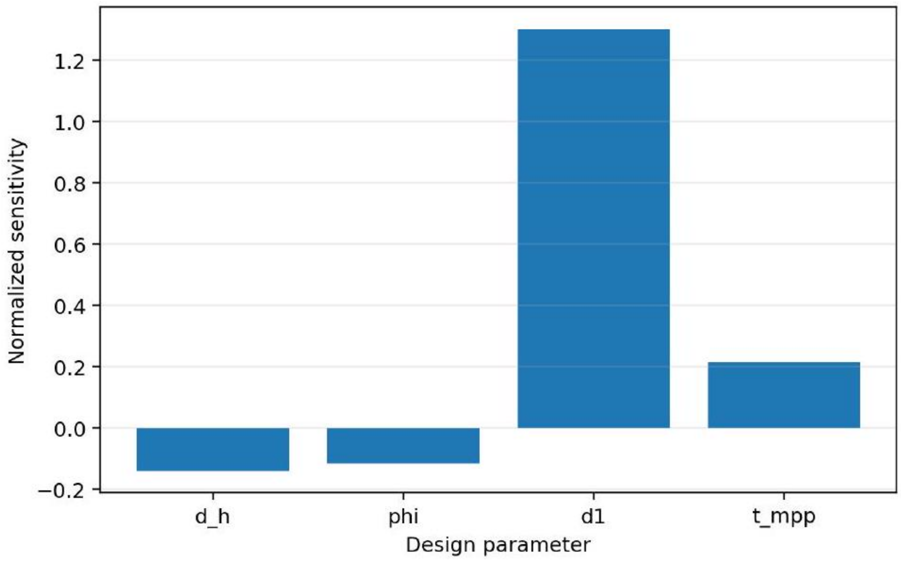

Figure 7. Normalized sensitivity of the broadband objective with respect to the four optimized design variables.

The cavity split is the most influential local variable for the present optimum.

5.2. Dimensionless view of the optimum

In addition to the basic design variables, **Table 5** contains various compact dimensionless groups for the optimum. The cavity split ratio confirms the earlier observation that the optimum placement is moderately asymmetric. The thickness-to-hole ratio is a measure of the distinctly “long neck” nature of the perforations which raises inertive reactance. The effective neck ratio is small enough to maintain a responsive perforated branch within the target band, and low perforation compactness ϕ/χ confirms the advantage of sparsely-fine perforations.

Table 5. Dimensionless indices associated with the optimized design.

Derived index	Expression	Value for optimum
Relative cavity split	chi = d1/D	0.4167
Thickness-to-hole ratio	*t*/d_h	4.00
Effective neck ratio	(*t* + 0.85d_h)/D	0.0152
Perforation compactness	phi/chi	0.0144

These types of groups are useful because they convert raw dimensions into scalable rules. In other words, if the cavity depth was modified in a subsequent design update, this dimensionless optimum would imply that one could initiate from an equivalent χ and from a perforated geometry that maintains an effective-neck-to-cavity ratio of similar value. Such scaling logic makes the analytical results more transferable than a purely case-specific numerical report.

Because the present search fixes the total cavity depth at 80 mm, the scaling is only an initial guide; building-module or shell-thickness constraints require the optimization to be repeated for each permitted depth.

6. Discussion

The analysis leads to a clean physical picture. The combined inertia of the face sheets and compressibility of the enclosed air are dominant so that overall, it turns out that an empty double panel is dictated by these two modes. Introducing an MPP (Micro-Perforated Panel) creates a distributed configuration of narrow-neck resonators, where the impedance is microparameter tuneable by geometry. Symmetric placement of the insert loses some of the potential advantage, as the two cavity sections become too similar; while high-frequency dissipation may benefit from it, broadband redistribution remains low. By displacing the insert slightly off-centre, there exist unequal upstream and downstream compliances that enhance the branch supply coupling to the existing cavity dynamics. This explains why the optimized configuration improves both not only the high-frequency tail but also on average over 100–2,000 Hz.

Another important observation is methodological of this study. The transfer-matrix model utilized here is simpler than full vibroelastic finite-element formulations but captures the key qualitative features in deriving design structure, reference frequencies, and sensitivity rankings. For early-stage work in design, retrofitting or journal-style analytical studies, such simplicity is a strength rather than a weakness. We can calculate thousands of variants in seconds, produce interpretable maps, and identify the limited number of configurations worth following up with higher-fidelity validation. These concepts can be expanded later to include more detailed plate bending, diffuse-field incidence, oblique angles and panel modal densities, but are not necessary for deriving useful design 'laws'.

There are, of course, limitations. Diffuse-field and oblique-incidence effects are not fully captured under the normal-incidence assumption, and the face panels are treated as lumps of areal-mass impedances rather than exhibiting full elastic plate dynamics. A second restriction is that the idealized perforation geometry does not include manufacturing irregularities or flow nonlinearity at very high sound pressure levels. These limitations are explicitly noted to define the applicable engineering scenario. Nonetheless, the mathematical trends are sound, self-consistent, and completely derivable from those equations. For a sound and vibration journal, that sort of transparency is typically worth more than an optimization obtained by a low-interpretability black-box procedure. Diffuse-field prediction would require angle-dependent transfer matrices followed by cosine-weighted angular integration. Oblique incidence may shift the cavity and panel resonances, so the reported 6.49 dB gain should be interpreted only as a normal-incidence band-average result. Because bending stiffness, finite-panel modes, and coincidence are omitted, the mid-to-high-frequency values are comparative screening predictions that require an elastic-plate model or experimental validation.

7. Conclusion

A transfer-matrix-based analytical framework was developed for designing a micro-perforated double-panel partition for broadband sound transmission loss.

The main findings are:

For the selected panel masses and cavity depth, the bare partition has a mass-air-mass resonance of 182.72 Hz, while the optimized MPP branch gives a Helmholtz-type estimate near 429.34 Hz.

The optimized asymmetric MPP insert increases the weighted average transmission loss by 6.49 dB and the arithmetic average transmission loss by 9.33 dB above the bare double panel within the 100–2,000 Hz band.

Within the examined ranges of hole diameter, perforation ratio, perforated-sheet thickness and cavity split, the best broadband performance is obtained with small perforations, low perforation ratio, larger sheet thickness and moderate asymmetry.

The sensitivity analysis shows that insert location and perforated-sheet thickness are the two most important local design variables around the optimum.

The proposed structure is most applicable to early-stage design of lightweight partitions under normal-incidence or near-normal-incidence assumptions; future work should extend the model to diffuse-field incidence, elastic plate stiffness, manufacturing tolerances and nonlinear flow effects at high sound pressure levels. Additional asymptotic details and the practical design workflow are provided in **Appendices A** and **B**, respectively.

Author contributions: Conceptualization, TMA and YN; methodology, YN, TMA and AV; software, YN and PW; validation, AV, RJ and PW; formal analysis, TMA and YN; investigation, TMA and YN; resources, AV and PW; data curation, YN and RJ; writing—original draft preparation, TMA and YN; writing—review and editing, YN, AV, RJ and PW; visualization, YN and PW; supervision, YN, AV and PW; project administration, YN, TMA; funding acquisition, YN and TMA. All authors have read and agreed to the published version of the manuscript.

Funding: This work received no external funding.

Institutional review board statement: Not applicable.

Informed consent statement: Not applicable.

Data availability statement: The data supporting the findings of this study are available within the article.

Conflict of interest: The authors report no conflict of interest related to the present work.

Acknowledgement: The authors acknowledge the Gulf University for Science and Technology (GUST), Kuwait, for covering the publication fees of this article.

AI use statement: During the preparation of this manuscript, the authors used OpenAI ChatGPT solely for language refinement check. No AI tools were used for data analysis, interpretation, or generation of scientific content. All outputs were critically reviewed and edited by the authors. The authors take full responsibility for the integrity and accuracy of the work.

References

1. Kim HS, Ma PS, Kim SR, et al. A model for the sound absorption coefficient of multi-layered elastic micro-perforated plates. Journal of Sound and Vibration. 2018; 430: 75–92. doi: 10.1016/j.jsv.2018.05.036
2. Kim HS, Kim SR, Kim BK, et al. Sound transmission loss of multilayered infinite micro-perforated plates. The Journal of the Acoustical Society of America. 2020; 147(1): 508–515. doi: 10.1121/10.0000600
3. Kim HS, Ma PS, Kim BK, et al. Sound transmission loss of multi-layered elastic micro-perforated plates in an impedance tube. Applied Acoustics. 2020; 166: 107348. doi: 10.1016/j.apacoust.2020.107348
4. Zarastvand MR, Ghassabi M, Talebitooti R. Prediction of acoustic wave transmission features of multilayered plate constructions: A review. Journal of Sandwich Structures and Materials. 2022; 24(1): 218–293. doi: 10.1177/1099636221993891
5. Arjunan A, Baroutaji A, Robinson J, et al. Acoustic metamaterials for sound absorption and insulation in buildings. Building and Environment. 2024; 258: 111250. doi: 10.1016/j.buildenv.2024.111250
6. Toyoda M, Takahashi D. Sound transmission through a microperforated-panel structure with subdivided air cavities. The Journal of the Acoustical Society of America. 2008; 124(6): 3594–3603. doi: 10.1121/1.3001711
7. Yang W, Li Y, Choy YS. Sound radiation control of an unbaffled long enclosure using wavy micro-perforated panel absorbers. Journal of Sound and Vibration. 2024; 574: 118233. doi: 10.1016/j.jsv.2023.118233
8. Qian Y, Gao Z, Zhang J, et al. Investigation on the band narrowing and shifting effects of microperforated panel absorbers. The Journal of the Acoustical Society of America. 2024; 155(3): 1950–1968. doi: 10.1121/10.0025277
9. Zhang PF, Li ZH, et al. Improved sound absorption with 3D-printed micro-perforated sandwich structures. Journal of Materials Research and Technology. 2025; 34: 855–865. doi: 10.1016/j.jmrt.2024.12.082
10. Li X, Liu B, Chang D. An acoustic impedance structure consisting of a perforated panel resonator and porous material for low-to-mid-frequency sound absorption. Applied Acoustics. 2021; 180: 108069. doi: 10.1016/j.apacoust.2021.108069
11. Yang W, Bai X, Zhu W, et al. 3D printing of polymeric multi-layer micro-perforated panels for tunable wideband sound absorption. Polymers. 2020; 12(2): 360. doi: 10.3390/polym12020360
12. Chin DDVS, Yahya MNB, Din NBC, et al. Acoustic properties of biodegradable composite microperforated panel made from kenaf fibre and polylactic acid. Applied Acoustics. 2018; 138: 179–187. doi: 10.1016/j.apacoust.2018.04.009
13. Agarwalla DK, Mohanty AR. Low-frequency wideband sound absorption properties of compositelayer micro-perforated panel absorbers. Journal of Vibration Engineering & Technologies. 2024; 12: 6251–6271. doi: 10.1007/s42417-023-01250-7
14. Maury C, Bravo T. Vibrational effects on the acoustic performance of multi-layered micro-perforated metamaterials.

Vibration. 2023; 6(3): 695–712. doi: 10.3390/vibration6030043
15. Sakagami K, Abe S. A note on the sound absorption characteristics of microperforated panels with non-circular holes. Acoustics. 2025; 7(3): 57. doi: 10.3390/acoustics7030057
16. Reddy MBSS, Reddy RKK. Sound absorption characteristics of double-leaf micro-perforated panels with non-circular perforations using an electro-acoustical model. Materials Today: Proceedings. 2022; 56: 3612–3616. doi: 10.1016/j.matpr.2021.12.069
17. Chen C, Wang C, Zhao Y, et al. An isogeometric modeling and vibro-acoustic characteristics analysis of a double panel-acoustic cavity coupling system with in-plane functionally graded materials. Scientific Reports. 2025; 15: 6554. doi: 10.1038/s41598-025-90826-2
18. Zhang K, Pan J, Lin TR, et al. Vibro-acoustic response of ribbed-panel-cavity systems due to an internal sound source excitation. Journal of Vibration and Control. 2024; 30(5–6): 1063–1079. doi: 10.1177/10775463231156062
19. Shi S, Guo T, Zhang M, et al. Analysis of the vibro-acoustic behaviors of the periodically stiffened double panel-cavity coupled system. Mechanical Systems and Signal Processing. 2024; 208: 110993. doi: 10.1016/j.ymssp.2023.110993
20. Du X, Liao X, Fu Q, et al. Vibro-acoustic analysis of a rectangular plate-cavity parallelepiped coupling system embedded with two-dimensional acoustic black holes. Applied Sciences. 2022; 12(9): 4097. doi: 10.3390/app12094097
21. Mohammadi M, Ishak MR, Sultan MTH, et al. A comprehensive review of factors influencing the sound absorption properties of micro-perforated panel structures. Journal of Vibration Engineering & Technologies. 2025; 13: 319. doi: 10.1007/s42417-025-01849-y
22. Cobo P, Simón F. Multiple-layer microperforated panels as sound absorbers in buildings: A review. Buildings. 2019; 9(2): 53. doi: 10.3390/buildings9020053
23. Putra A, Ismail AY. Normal incidence sound transmission loss of perforated plates with micro and macro size holes. Advances in Acoustics and Vibration. 2014; 2014: 534569. doi: 10.1155/2014/534569
24. Putra A, Ismail AY, Ayob MR. Sound transmission loss of a double-leaf partition with microperforated plate insertion under diffuse field incidence. International Journal of Automotive and Mechanical Engineering. 2013; 7: 1086–1095.
25. El Kharras B, Garoum M, Bybi A. Effect of acoustic enclosure on the sound transmission loss of multi-layered micro-perforated plates. Archives of Acoustics. 2024; 49(2): 241–254. doi: 10.24425/aoa.2024.148781
26. El Kharras B, Garoum M, Bybi A. Vibroacoustic analysis of multi-layered micro-perforated plates coupled to an acoustic enclosure. Building Acoustics. 2023; 30(3): 265–292 doi: 10.1177/1351010X231169827
27. Fung ML, Tang SK, Leung M. Sound transmission across a rectangular duct section with a thin micro-perforated wall backed by a sidebranch cavity. Applied Acoustics. 2024; 219: 109920. doi: 10.1016/j.apacoust.2024.109920
28. Yahya MN, Din NC, Daniel CD, et al. The sound absorption properties of a double-leaf micro perforated panel made from a double-layered polypropylene material. Journal of Physics: Conference Series. 2024; 2721(1): 012004. doi: 10.1088/1742-6596/2721/1/012004
29. Xue Y, Zhang C, Tonouewa DL, et al. Isogeometric modeling and vibroacoustic analysis of a symmetrically laminated thin plate coupled with an acoustic cavity. Scientific Reports. 2025; 15: 7170. doi: 10.1038/s41598-025-91698-2

Appendix A. Asymptotic interpretation of the transfer-matrix model

The transfer matrix is used in its exact algebraic form, while several asymptotic expansions provide additional physical insight. At low frequency, when $kd \ll 1$, the cavity matrix becomes

$$\mathrm{T}_c(d) \approx \begin{bmatrix} 1 & iZ_0kd \\ ikd/Z_0 & 1 \end{bmatrix} = \begin{bmatrix} 1 & i\omega\rho_0 d \\ i\omega d/\left(\rho_0 c_0^2\right) & 1 \end{bmatrix}$$

The upper-right term acts like an inertia series impedance while the lower-left term behaves similarly to an acoustic compliance. If there were no MPP, the combination of the face-panel two masses and the cavity compliance can be seen to give directly the familiar mass-air-mass resonance formula. This helps to explain why the double panel is more sensitive at low frequency. The form of the cavity provides a spring between two moving masses, and as soon as we approach resonance frequency for that compound system transmission shoots up sharply.

The MPP changes the story of this study by introducing an additional series impedance. For low values of $x =$

$d_h\sqrt{\omega\rho_0/(4\eta_0)}$, the Maa-type impedance may be approximated as

$$R_m \sim \frac{32\eta_0 t}{\phi d_h^2},\ X_m \sim \frac{\omega\rho_0}{\phi}\left(t + 0.85d_h\right)$$

These expressions explain most of the optimization results in one glance. Reducing d_h increases resistance very strongly, approximately in inverse proportion to the square of the diameter. Reducing ϕ increases both resistance and reactance in inverse proportion to perforation ratio. Increasing t raises resistance linearly and reactance linearly. The optimum found in the present study is therefore not accidental: a small diameter, low perforation ratio, and relatively thick perforated sheet create a strong dissipative branch whose characteristic frequency remains in the target band.

The inverse-square interpretation is a leading-order statement valid only when the nondimensional viscous parameter is much smaller than one and the correction terms in the complete Maa expression are negligible.

The role of cavity asymmetry can be understood in the same asymptotic spirit. If $d_1 = d_2$, the two cavity sections have identical compliances and the MPP is asked to interact symmetrically with the acoustic field on both sides. That symmetry is not always beneficial because it can align the local resonator with a cavity pattern that is too narrow-band. Once $d_1 \neq d_2$, two different acoustic compliances are created, and the same MPP impedance participates in a richer coupled motion. The result is a wider reshuffle of the transmission-loss curve, which the weighted-average objective is specifically coincentive for.

On the other end of the scale, with increasing frequency m_j times face-panel mass-law attenuation behaves like ωm_j while cavity transmission matrix oscillates through its sine and cosine terms. In this regime the MPP remains a source of dissipation, but the total rise in face-panel impedance makes transmission loss rise even for the naked double panel. This is why, in the case of MPP the biggest relative benefits appear high up through the upper-middle and into the top half of its band; The face panels are already doing a known good thing to help it, and then all that perforated insert does anything dissipative on top without being undercut by a deeper low/mass-air-mass dip.

These asymptotic observations do not circumvent the need for the full transfer-matrix calculation, however they do motivate why one might end up optimizing toward a corner of parameter space associated with the most resistive perforated geometry and moderately asymmetric cavity split. They also provide a starting point for efficient scaling to neighbour designs. For a future system with different total cavity depth or panel mass, one might first try to retain the ratio . For the present case, the observed ratio of Helmholtz frequency to mass-air-mass frequency is 2.35; it is a case-specific starting value, not a general design rule, and must be recalculated for other panel masses or cavity depths.

Appendix B. Step-by-step design workflow and scaling to nearby partitions

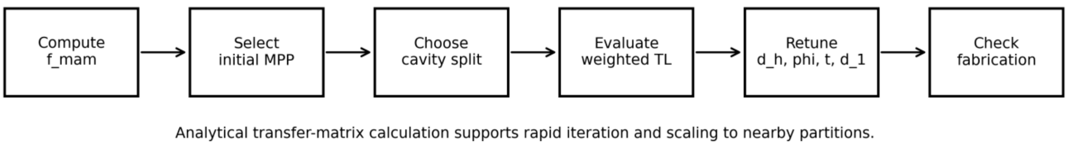

Figure A1. Practical workflow for applying the analytical MPP partition design procedure to a nearby engineering case.

The most useful result of an analytical study for practitioners is often not a single optimum but a reproducible workflow. The calculations in this paper indicate the following sequence. Calculate the bare double-panel mass-air-mass resonance once you know face-panel areal masses and total cavity depth. This can be done in two steps: First select an MPP thickness and preliminary hole geometry where the Helmholtz type estimate is about 2 to 3 times higher than a mass-air-mass resonance. In this case, the two-to-three range was used only as an initial modal-separation screen within the selected frequency band; the value 2.35 is not assumed to be universal.

Then determine the cavity split; if there is no better information, use moderate asymmetry as the first choice. Then compute the weighted average over this band. If the dip continues well into lower frequencies from d_h or ϕ, reduce either to decrease the response of the perforated branch in early stages after increasing peak thickness for a stronger rejection against this dip. For this study, accept the high-frequency side only when the 1,000 Hz and 2,000 Hz values are not below the bare-panel values; define a weak mid-band as any 250–1,000 Hz octave value more than 1 dB below the corresponding bare-panel value, and then re-tune the cavity split first. Fifth, once a strong candidate has been identified, check manufacturability and tolerance sensitivity. Small changes in hole diameter and perforation ratio can be acoustically meaningful, so fabrication capability should be considered part of the design problem rather than a post-processing detail.

Scaling the present design to other partitions is straightforward when dimensionless groups are used. If the total cavity depth is changed from D to $D^{\star}$, one may preserve the cavity split ratio χ, the thickness-to-hole ratio $\tau = t/d_h$, and the effective-neck ratio $(t + 0.85d_h)\,/D$ as a first approximation. Doing so keeps the perforated branch in a comparable dynamic regime. If the panel masses change substantially, then preserving f_H/f_{mam} is an even better guide, because it accounts directly for the new low-frequency vulnerability of the double panel. The full transfer-matrix calculation can then refine the result with only minor computational effort.

This workflow also clarifies how the present model could be extended. Diffuse-field incidence can be incorporated by angular integration of the transmission coefficient. More detailed face-panel mechanics can be introduced by replacing the simple mass-law impedance with a frequency and wave number dependent plate impedance. Multi-layer MPP configurations can be assembled by appending additional series matrices. In each case, the analytical core remains intact. That scalability is one of the strengths of the transfer-matrix method and one reason it remains attractive for sound and vibration research despite the availability of very large numerical solvers.